ASRL TR 130-1

THE RESPONSE AND AIRLOADING OF HELICOPTER ROTOR BLADES DUE TO DYNAMIC STALL

by

Wayne Johnson

MASSACHUSETTS INSTITUTE OF TECHNOLOGY
AEROELASTIC AND STRUCTURES RESEARCH LABORATORY
CAMBRIDGE, MASSACHUSETTS 02139

May 1970

UNITED STATES ARMY RESEARCH OFFICE-DURHAM
CONTRACT NUMBER DA-31-124-ARO-D-247

4846.11-E

ASRL TR 130-1

THE RESPONSE AND AIRLOADING OF HELICOPTER ROTOR BLADES DUE TO DYNAMIC STALL

by

Wayne Johnson

Massachusetts Institute of Technology
Aeroelastic and Structures Research Laboratory
Cambridge, Massachusetts 02139

May 1970

This work was sponsored by the United States Army Research Office-Durham, under Contract Number DA-31-124-ARO-D-247.

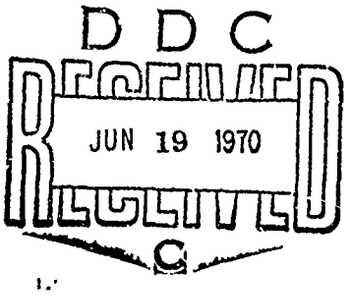

ABSTRACT

An aerodynamic model is constructed for the application of the properties of dynamic stall of airfoils to the calculation of the airloads and blade motion of helicopter rotor blades. Dynamic stall occurs on an airfoil undergoing pitching motion at high angle of attack, and is characterized by peak section lift and moment much larger than the corresponding static stall loads. A method is developed for the solution of the equations of motion of a rotor blade by means of harmonic analysis. The effect of dynamic stall on the blade torsional motion at high advance ratio is examined, and comparison is made with the limited experimental data available. An increase in the dynamic stall angle is shown to significantly decrease the amplitude of the pitch motions.

CONTENTS

LIST OF ILLUSTRATIONS

NOMENCLATURE

a_o	lift curve slope
b	blade semichord
c_d	section drag coefficient
c_l	section lift coefficient
c_m	section moment coefficient
D	Drag
i	angle between tip path plane and the forward velocity; positive for rearward tilt of the thrust
i	imaginary number: $\sqrt{-1}$
L	Lift
M	Moment
r	blade spanwise variable
R	Rotor radius
α	section angle of attack
$\dot{\alpha}^{(s)}_{c/V}$	nondimensional rate of change of angle of attack, at the instant of stall
β	blade flapping angle
θ	blade pitch angle
μ	rotor advance ratio: forward speed divided by ΩR
ρ	fluid density
ψ	rotor azimuthal variable
Ω	rotor rotational speed

BLANK PAGE

SECTION 1

INTRODUCTION

The large transient control loads encountered at high forward speeds or high blade loadings remain a significant problem in the operation and design of helicopters. A primary source of these loads is the aerodynamic moment due to blade stall. Results of an investigation into the nature and effects of stall in the aerodynamic environment characteristic of helicopter blades (References 1 to 4) indicate that the stall phenomenon exhibited by an airfoil undergoing a rapidly changing angle of attack, known as dynamic stall, differs substantially from the familiar static stall at constant angle of attack. Such a situation of rapidly increasing angle of attack characterizes a helicopter rotor blade as it traverses the rotor disc, particularly on the retreating side of the disc at high advance ratios. This report presents a method which was developed to calculate the aerodynamic loading and resulting blade motion of a rotor blade, particularly the aerodynamic moment and resulting blade torsional motion due to dynamic stall. The aerodynamic model developed was specifically designed for high forward speeds ($\mu > 0.25$), where a simple wake geometry model is accurate. Moreover, due to the lack of symmetry over the rotor disk at high forward speed, recurrent entry to and exit from stall (stall flutter) is not likely to occur, and the very complicated and detailed wake and aerodynamics due to such a motion need not be considered.

In what follows all quantities are nondimensional, based on the fluid density, the rotor radius, and the rotor rotational speed (ρ, R, Ω). The section lift, moment, and drag coefficients are conventionally defined.

SECTION 2

THE AIRLOADS AND BLADE MOTION CALCULATION

The calculation procedure used to determine the airloads and blade motion of a helicopter rotor blade follows a reference blade around the azimuth in discrete steps $\Delta\Psi$ of the order of ten degrees. The downwash at several blade stations, the section loading at several blade stations, the blade motion, and the wake geometry changes are calculated successively; then the blade is moved to the next azimuth station. This procedure is illustrated in Figure 1. The use of a variable inflow calculated on the basis of a wake of trailed and shed vorticity precludes any closed form solution. The calculations are therefore performed iteratively until they converge to the steady state solution. The solution is determined by the physical properties of the blade (the semi-chord to span ratio b, the Lock number L.N., and others), and by the root collective pitch θ_o^o, the tip path plane inclination angle i, the advance ration μ, and the tip Mach number $M_{1.0,90}$.

2.1 The Aerodynamic Loading

The section lift, moment, and drag -- L, M, D -- are determined from the appropriate aerodynamic theory based on the state of the flow and the blade motion. The state of the flow (attached or nonattached) at a certain blade station is determined by the past history of the flow and by the angle of attack α:

$$\alpha = \theta - \tan^{-1} \frac{U_P}{U_T}$$

where

$$U_T = r + \mu \sin\Psi$$

$$U_P = \lambda + \dot{z} + \mu \frac{\partial z}{\partial r} \cos\Psi$$

$$= \lambda + r\dot{\beta} + \eta\dot{q} + \mu\left(\beta + q\frac{\partial \eta}{\partial r}\right)\cos\Psi$$

(with the convention that a positive angle of attack in the reverse flow region corresponds to a downward acting lift). The state of the flow is determined as follows:

(a) For $|\alpha|$ less than a defined stall angle, the flow is considered attached. The loads are determined using lifting line and lifting surface theories.

(b) When $|\alpha|$ becomes greater than some α_{DS}, the section is considered to stall dynamically. The loads are determined by the parameter $\dot{\alpha}c/V$ at the instant of stall. The dynamic stall state lasts until the section angle of attack begins to decrease (but at least for an interval $\Delta\psi_{RT}$), and then the flow is considered separated. During the separated state the loads decay from the dynamic stall values to static stall values. When $|\alpha|$ next goes below some α_{SS} the flow becomes attached again.

(c) When $|\alpha|$ becomes greater than some α_F the flow is called feathered (typically α_F = 60 degrees). When $|\alpha|$ next goes below α_F, the flow is considered statically stalled, until $|\alpha|$ goes below α_{SS} and the flow reattaches.

The only feature of the reverse flow region which is considered is the direction of the component of the velocity u_T normal to the span direction. This determines the double sign:

$$\pm = \text{sign}(u_T) = \text{sign}(r + \mu \sin\psi)$$

which will occur frequently below. Several additional points must be considered:

(a) For points too near the reverse flow boundary ($u_T = 0$) the loading is set to zero.

(b) For radial stations which at the last azimuth station were on the other side of the reverse flow boundary, so that the past history of the flow is not well defined by the above model, the flow is considered to have been attached at the last azimuth station. Whatever the state of the flow is near the reverse flow boundary, the loading will be small because of the low dynamic pressure of the velocity normal to the span.

(c) If the angle of attack changes sign in the separated region, so that a more detailed calculation along the azimuth would show the section flow reattaching and then restalling as the angle of attack goes through zero, the section is considered to be statically stalled.

The logic described above is shown in Figure 2. This model is designed to show the effects of a rather impulsive loading (due to dynamic stall) on the torsional motion of a blade under high loading conditions and high advance ratio. It is not appropriate for handling several successive excursions in and out of stall unless an impractically small azimuth step $\Delta\Psi$ is used.

The convention for the positive directions of the loads is as follows:

lift, L	upward
moment, M	nose up, about the quarter chord (the feathering axis)
drag, D	opposing the blade rotation
pressure, $-\Delta p$	upward
circulation, Γ	directed outward along the blade

2.1.1 Attached Flow

For the blade section in attached flow, the loading is calculated using lifting line theory; that is, the flow is considered locally two-dimensional, with the influence of the rest of the blade and the rotor wake represented by just a downwash velocity at the blade section. The aerodynamic loading is due to the blade motion and the wake induced downwash. The downwash is calculated from the trailed and shed vorticity in the wake of each blade of the rotor. In early calculations, only the downwash due to the trailed vorticity was calculated in this manner; the effect of the shed vorticity behind the reference blade was accounted for by the use of Theodorsen's lift deficiency function. The two methods of handling the shed vorticity showed little difference as far as stall loads and blade motion were concerned.

As a first order correction for compressibility effects, the Prandtl-Glauert factor is used, based on the Mach number of the flow normal to the span of the blade. Thus

$$\frac{L}{4\pi b} = \frac{1}{\sqrt{1-M_N^2}} \left(\frac{L}{4\pi b}\right)_{\text{incompressible lifting line theory}}$$

$$\frac{M}{4\pi b} = \frac{1}{\sqrt{1-M_N^2}} \left(\frac{M}{4\pi b}\right)_{\text{incompressible lifting line theory}}$$

where

$$M_N = M_{1.0,90} \frac{|r+\mu \sin\psi|}{r_T+\mu}$$

$M_{1.0,90}$ = Mach number of tip ($r = r_T$) at ψ = 90 degrees

2.1.2 Nonattached Flow

The aerodynamics of the flow when it is stalled, separated, or feathered give the section load coefficients -- c_l, c_m, c_d -- for lift positive upward, moment (about the feathering axis) positive nose upward, and drag positive in the direction opposing the relative velocity. The lift and drag, L* and D*, are respectively perpendicular to and in the direction of the actual section relative velocity (see Figure 3). Converting these coefficients to loads based on Ω and R gives

$$L^* = u_T^2 b c_l / \sqrt{1 - M_N^2}$$

$$M = u_T^2 2b^2 c_m / \sqrt{1 - M_N^2}$$

$$D^* = u_T^2 b c_d$$

Referring again to Figure 3, the loads can be converted to lift and drag in the no feathering plane using

$$L = L^* \frac{|u_T|}{\sqrt{u_T^2 + u_P^2}} - D^* \frac{u_P}{\sqrt{u_T^2 + u_P^2}}$$

$$D = D^* \frac{u_T}{\sqrt{u_T^2 + u_P^2}} + L^* \frac{\pm u_P}{\sqrt{u_T^2 + u_P^2}}$$

These expressions are necessary because of the large angles which may be involved in nonattached flow. The circulation is given by

$$\Gamma = \frac{a_o}{2\pi} \frac{1}{u_T} L^*$$

and the actual loads by $a_o/2\pi$ times L and M (for use in the equations for the blade motion however, the lift curve slope correction factor is already included in the Lock number).

2.1.3 Dynamic Stall

The loss of lift and circulation and the shift of center of pressure an airfoil at an angle of attack above the static stall angle α_{SS} (generally about 8 to 12 degrees) are familiar aerodynamic phenomena. The operation of a helicopter rotor blade in an environment of high loading and changing angle of attack makes it necessary to consider stall as a dynamic rather than a static phenomenon. The unsteady aerodynamics involved in dynamic stall are not yet completely understood (see References 1 to 4) but fundamental to characterizing the problem is the time scale of the airfoil motion, as represented by the parameter $\dot{\alpha}c/V$. The primary characteristics of dynamic stall are its occurrence at an angle of attack greater than the static stall angle, followed by the shedding of vorticity from the leading and trailing edges. The unsteady aerodynamic forces due to the vorticity passing over the upper surface of the airfoil produce a lift and nose down moment, with peak values much greater than the corresponding static stall loads. Experimental and theoretical work (Reference 4) has shown that the primary parameter of dynamic stall is the rate of change of angle of attack at the instant of stall, in the non-dimensional form

$$\frac{\dot{\alpha}^{(s)}c}{V} = \left| \frac{\left(\frac{\Delta\alpha}{\Delta\psi}\right)2b}{u_T} \right|$$

with little dependence on the actual angle of dynamic stall. Figure 4 shows the results of both theory and experiment for the variation with $\dot{\alpha}^{(s)}c/V$ of the peak lift and moment coefficients, $c_{l_{max}}$ and $c_{m_{max}}$. Although still requiring experimental verification, the theory of Reference 4 implies that the peak coefficients approach limits of the order of 3.0 for $c_{l_{max}}$ and -0.8 for $c_{m_{max}}$ for high stall rates.

As a model for dynamic stall, it is assumed that above a given angle of attack, α_{DS}, as long as the angle of attack is increasing, the lift and moment coefficients are maintained at constant values. These coefficients are taken as equal to the peak coefficients as given by the experimental and theoretical results cited aobve, and are therefore dependent on the stall rate parameter $\dot{\alpha}^{(s)}c/V$. The empirical representation used is also shown in Figure 4. Data (Reference 4) indicate that the dynamic stall angle is about 14 to 20 degrees; typically the value of α_{DS} = 15 degrees is used. Thus the value of $\dot{\alpha}^{(s)}c/V$ at the instant of stall gives

$$c_{\ell_o} = \pm \text{sign}(\alpha)\, c_{\ell_{max}}(\dot{\alpha}^{(s)}c/V)$$

$$c_{m_o} = \text{sign}(\alpha)\, c_{m_{max}}(\dot{\alpha}^{(s)}c/V) + \left(-\tfrac{1}{2} \pm \tfrac{1}{2}\right) c_{\ell_o}$$

The use of this model (Reference 5) has shown that typically the large nose down moment generated by dynamic stall quickly causes the angle of attack to begin to decrease (due to elastic pitch motion of the blade) and thus the flow to enter the separation model. The dynamic stall region extends only for about $\Delta\Psi$ = 15 degrees. The resultant elastic pitch excitation is characteristically very impulsive. At high advance ratios the model is only weakly dependent on the stall angle α_{DS}. The possibility of self-excited elastic torsional motions (stall flutter) is likely only at very low advance ratio, with a great deal of symmetry around the rotor disk. At very high advance ratios ($\mu > 0.5$), the value of $\dot{\alpha}^{(s)}c/V$ is frequently larger than the range shown in Figure 4, and so the dynamic stall loads are very large.

The use of harmonic analysis to represent the load data, which is calculated only at discrete azimuth points, as a smooth

distribution around the disk actually replaces the instantaneous rise of the stall loads to the peak dynamic stall values by a gradual increase, with the rise time determined by the azimuth increment in the harmonic analysis (see Section 2.5.2). For a very small azimuth increment in the calculation process, some limit must be placed on the rate of increase of the stall loads. Using a linear rise, the lift and moment coefficients are

for $\Delta\Psi < \Delta\Psi_{RT}$

$$c_\ell = (c_{\ell_o} - c_{\ell_a}) \frac{\Delta\Psi}{\Delta\Psi_{RT}} + c_{\ell_a}$$

$$c_m = (c_{m_o} - c_{m_a}) \frac{\Delta\Psi}{\Delta\Psi_{RT}} + c_{m_a}$$

and for $\Delta\Psi > \Delta\Psi_{RT}$

$$c_\ell = c_{\ell_o}$$

$$c_m = c_{m_o}$$

where c_{l_a} and c_{m_a} are the coefficients for the attached flow at the dynamic stall angle and $\Delta\Psi$ is the azimuth increment since the dynamic stall angle was reached. The experimental and theoretical data (Reference 4) suggest that the rise time $\Delta\Psi_{RT}$ should be approximately 10 degrees, which is also confirmed by a comparison of the results of this calculation model and experimental data.

2.1.4 Separation

Experimental results (Reference 6) show that the flow over an airfoil oscillating at high angle of attack separates at the peak angle of attack for values of the reduced frequency, $k = \omega b/V$, greater than 0.3. It is also shown there that the Theodorsen theory of oscillating airfoils is equivalent to a first order differential equation for the moment coefficient of the form

$$\frac{\partial}{\partial x}(c_m - c_{m_i}) + \frac{1}{T_m}(c_m - c_{m_i}) = \frac{\lambda}{T_m}\alpha$$

where the subscript i refers to the initial conditions, and the Theodorsen theory gives λ and the time constant T_m as functions of k and C(k) (the lift deficiency function). A similar expression may be derived for the lift coefficient, with a time constant T_l. When this equation was assumed to hold in the stalled region also, moment variation with angle of attack was calculated which was in good agreement with the experimental results. Since a first order equation would be expected to give a reasonable approximation to the decay of the dynamic stall loads (see Reference 3 for experimental data for this decay) this agreement primarily indicates that the time constants given by the Theodorsen theory may also be used when the airfoil is stalled.

Therefore as a model for separated flow, it is assumed that after the section angle of attack reaches its maximum value, the lift and moment coefficients decay exponentially to static stall values. Thus the lift and moment coefficients are

$$c_\ell = (c_{\ell_o} - c_{\ell_s})\, e^{-(\Psi-\Psi_o)\frac{r}{b\tau_L}} + c_{\ell_s}$$

$$c_m = (c_{m_o} - c_{m_s})\, e^{-(\Psi-\Psi_o)\frac{r}{b\tau_M}} + c_{m_s}$$

where c_{l_o} and c_{m_o} are the coefficients at the peak angle of attack (dynamic stall coefficients) and c_{l_s} and c_{m_s} are the static stall coefficients (based on the same sign(α) and sign(u_T) as are c_{l_o} and c_{m_o}); Ψ_o is the azimuth angle at which the separation region was entered. The time constants are given by the Theodorsen theory as approximately $\tau_L = 1.0$ and $\tau_M = 2.5$. Calculations with these values show that the time constants used for the transient stall of the rotor blade should be several times these values, which were derived and experimentally confirmed for a highly periodic stalling motion.

Dynamic stall as described above is a phenomenon rather independent of the airfoil motion after its initiation at the dynamic stall angle. Thus the dynamic stall state should exist for a definite period, regardless of the subsequent blade motion. Therefore the separation state is assumed not to start until at least $\Delta\psi_{RT}$ after the dynamic stall angle is reached; if the angle of attack is still increasing after this point, the separation state begins when the angle of attack starts to decrease.

It is assumed that the flow reattaches at the static stall angle α_{SS}. However, reattachment is also delayed if necessary until $\Delta\psi_{RT}$ after the initiation of dynamic stall.

2.1.5 Static Stall

The model used for static stall assumes that the lift and moment coefficients are maintained at the constant static stall values, c_{l_s} and c_{m_s}. Then the coefficients are

$$c_l = \pm \text{sign}(\alpha)\, c_{l_s}$$

$$c_m = \text{sign}(\alpha)\, c_{m_s} + \left(-\tfrac{1}{2} \pm \tfrac{1}{2}\right) c_l$$

Typical values used are $c_{l_s} = 1.0$ and $c_{m_s} = -0.15$, and for the static stall angle $\alpha_{SS} = 12$ degrees.

2.1.6 Feathered Flow

The experimental results of Reference 7 show that the stall model is reasonably accurate up to angles cf attack of around 60 degrees. These experiments were static measurements on a NACA 0012 airfoil section. A good approximation to the experimental coefficients above the feathered angle is given by

$$c_l = \pm \text{sign}(\alpha)\, c_{l_f}\, \frac{90^\circ - |\alpha|}{90^\circ - \alpha_F}$$

$$c_m = \text{sign}(\alpha)\, c_{m_f}$$

for $|\alpha| > \alpha_F$. The experiments give the parameters: $c_{l_f} = c_{l_s} = 1.0$; $c_{m_f} = -0.40$; and $\alpha_F = 60$ degrees.

2.1.7 The Drag

The experimental data of Reference 7 also give the drag coefficient for the NACA 0012 airfoil section. Unlike for attached flow, for nonattached flow the drag may have a significant component in the rotor thrust direction because of the large local angle of attack. For nonattached flow, the data is approximated quite well by:

$$c_d = 2.0 (\sin\alpha)^2$$

2.2 The Rotor Wake and Downwash

The wake of a helicopter rotor blade in forward flight consists of trailed and shed vorticity in a distorted, skewed, helix. In order to calculate the downwash induced at the rotor blade by this wake, it is represented by a net of finite strength, finite length line vortices behind each blade. The distribution of the blade bound circulation over the rotor disk, $\Gamma(r,\psi)$, is sufficient to establish, by continuity of vortex lines, the strength of each line element in the net. A semi-rigid wake geometry model is used to give the position of each line element; that is, each point of the wake is assumed to travel downward always at a velocity equal to the downwash at the point on the disk from which it was trailed or shed. From its strength and position, the downwash induced by each line element may be calculated; the downwash at the rotor blade is then the sum of the contributions from all elements in the wake.

2.3 The Reverse Flow Region

It is shown in Reference 7 that an airfoil in reverse flow has almost the same lift and moment variation with angle of attack

as for conventional flow, as would be expected with thin airfoils. Therefore the only change in the model is in the positive directions of the loads. As far as the blade torsional motion is concerned, the most important feature of the reverse flow region is that the aerodynamic center is then at the three-quarter chord, so the lift gives a large moment about the blade feathering axis, normally located at the quarter chord.

2.4 Compressibility effects

The only consideration of compressibility effects on the loads is the use of the Prandtl-Glauert correction factor based on the Mach number of the local velocity perpendicular to the span, u_T. The neglect of the effect of compressibility on the stall loads is a serious defect, as it is well established that this is a significant factor for airfoils stalling in the environment characteristic of helicopter blades. However, once experimental and theoretical data on the effects of compressibility on dynamic stall become available, it should be easy to incorporate them into the aerodynamic model which has been described here.

2.5 The Blade Motion

The vertical position of the blade is composed of the feathering axis deflection, z_o, and a chordwise rigid pitch motion, θ:

$$z_b = -z_o(r,\psi) + x\,\theta(r,\psi)$$

The deflection of the elastic axis is represented as the sum of rigid flapping and first mode elastic bending; and the pitch motion as the sum of a rigid (spanwise) pitching mode and first mode elastic pitching:

$$z_o = r\beta(\psi) + \eta(r)\,q_T(\psi)$$

$$\theta = \theta(\psi) + \xi(r)\,\theta_{tw}(\psi)$$

where $\xi(0) = 0$. An approximate mode shape is used for elastic bending, and the elastic mode is typically linear twist:

$$\eta(r) = 4r^2 - 3r$$

$$\xi(r) = r$$

The equation of motion is most conveniently solved in the no feathering plane, where the only control input is collective pitch (the tip path inclination angle i also enters indirectly through the downwash). Cyclic pitch can be varied arbitrarily with the orientation of the shaft; the dynamics and aerodynamics of the rotor determine the orientation of the no feathering plane with respect to the tip path plane.

2.5.1 The Equations of Motion

The equations of motion for a constant chord (uniform spanwise structural properties), coincident elastic axis and inertial axis, articulated (no lag hinge, zero flapping hinge offset) blade may be derived following Reference 8:

$$\ddot{\beta} + \beta = L.N. \int_{r_R}^{r_T} r \frac{L}{4\pi b} dr$$

$$I_2 (\ddot{q}_\gamma + \gamma_2^2 q_\gamma) = L.N. \int_{r_R}^{r_T} \eta \frac{L}{4\pi b} dr$$

$$I (\ddot{\theta} + \theta + \omega_o^2 (\theta - \theta^*)) + S_{tw} (\ddot{\theta}_{tw} + \theta_{tw}) = L.N. \int_{r_R}^{r_T} \frac{M}{4\pi b} dr$$

$$I_{tw} (\ddot{\theta}_{tw} + \theta_{tw} + \omega_{tw}^2 (\theta_{tw} - \theta^*_{tw})) + S_{tw} (\ddot{\theta} + \theta) = L.N. \int_{r_R}^{r_T} \xi \frac{M}{4\pi b} dr$$

where

$$I_b = \int_0^{r_T} r^2 m \, dr$$

I_θ = blade section moment of inertia about the feathering axis

$$I_2 = \frac{1}{I_b} \int_0^{r_T} \eta^2 m \, dr \cong 0.6$$

$$I = \frac{1}{I_b} \int_0^{r_T} I_\theta \, dr \cong \frac{4}{10} b^2$$

$$I_{tw} = \frac{1}{I_b} \int_0^{r_T} \xi^2 I_\theta \, dr = I \int_0^{r_T} \xi^2 \, dr$$

$$S_{tw} = \frac{1}{I_b} \int_0^{r_T} \xi I_\theta \, dr = I \int_0^{r_T} \xi \, dr$$

$L.N.$ = Lock number = $\frac{\rho a_0 c R^4}{I_b}$

ν_2 = elastic bending frequency $\cong$ 2.7/REV

ω_0, ω_{tw} = nonrotating natural pitch frequencies

θ° = collective pitch input

θ°_{tw} = structural twist

The lift and moment, L and M, are based on the ideal lift curve slope 2π; the Lock number includes the lift curve slope correction factor.

The pitching equations of motion are very sensitive to impulsive moment excitation, and in order to obtain a convergent solution by means of harmonic analysis, it is necessary to include

part of the aerodynamic damping on the left hand side of the equations. Thus the nonharmonic (no dependence on Ψ), incompressible damping is extracted from the lifting line result for the aerodynamic moment. To the total (compressible) moment, $M/4\pi b$, is added the quantity:

$$\frac{1}{4\pi b}\, r\pi b^3 \ddot{\theta}$$

or

$$\frac{1}{4\pi b}\, r\pi b^3 \xi \ddot{\theta}_{tw}$$

for the equations of motion for θ and θ_{tw} respectively. Correspondingly to the left hand side of the equations are added the terms:

$$I D \dot{\theta}$$

and

$$I_{tw} D_{tw} \dot{\theta}_{tw}$$

where

$$D = \frac{L.N.}{8} \frac{b^2}{I} \int_{r_R}^{r_T} 2r\,dr$$

$$D_{tw} = \frac{L.N.}{8} \frac{b^2}{I_{tw}} \int_{r_R}^{r_T} 2r\xi^2\,dr$$

(The damping terms given here are for the feathering axis at the aerodynamic center only.)

2.5.2 Solution for the Blade Motion

The equations of motion are most conveniently solved by harmonic analysis of the loads and blade motion. Thus writing

$$\beta = \sum_{n=-\infty}^{\infty} \beta_n e^{in\Psi}$$

and similarly decomposing q, θ, θ_{tw}, θ°, θ°_{tw}, and the integrals of the lift and moment, the equations of motion become:

$$\beta_n (1-\nu^2) = L.N. \left(\int_{r_R}^{r_T} r \frac{L}{4\pi b} dr \right)_n$$

$$q_f^n I_z (\nu_z^2 - \nu^2) = L.N. \left(\int_{r_R}^{r_T} \nu \frac{L}{4\pi b} dr \right)_n$$

$$\theta_n I (\omega_o^2 + 1 - \nu^2 + D_{in}) + \theta_{tw_n} S_{tw} (1-\nu^2)$$
$$= \theta_n^\circ I \omega_o^2 + L.N. \left(\int_{r_R}^{r_T} \frac{M}{4\pi b} dr \right)_n$$

$$\theta_{tw_n} I_{tw} (\omega_{tw}^2 + 1 - \nu^2 + D_{tw_{in}}) + \theta_n S_{tw} (1-\nu^2)$$
$$= \theta^\circ_{tw_n} I_{tw} \omega_{tw}^2 + L.N. \left(\int_{r_R}^{r_T} \frac{M}{4\pi b} dr \right)_n$$

All but the steady components (n = 0) of the collective and twist inputs, θ° and θ°_{tw}, are usually zero. These equations are easily solved for the harmonics of the blade motion.

The right hand sides of these equations are the harmonics of the integrals over the span of the aerodynamic forcing loads. In the calculation of rotary wing airloads these integrals will be evaluated only at a finite number of azimuth stations around the disk. Calling any of these integrals $F(\Psi)$, its value F_j is calculated at J azimuth stations. Then the harmonics of F are:

$$F_n = \frac{1}{J} \sum_{\text{azimuth}} F_j e^{-in\Psi_j} \quad , \quad \Psi_j = j \frac{2\pi}{J}$$

so that

$$F(\Psi) \cong \sum_{n=-N}^{N} F_n e^{in\Psi} \quad , \quad N \leq J/2$$

For N = J/2 this gives exactly $F(\Psi_j) = F_j$; for N < J/2 this is an approximation in the least squares sense.

Because of the smoothing nature of the harmonic representation, the rate of change of a function between two calculated points will be several times the rate of change of a straight line representation between the two points. This can introduce convergence problems when large changes in the loads are involved, as when stall occurs, because the effective rise time of the loads is increased. Therefore all the harmonics, F_n, are multiplied by the factor:

$$\left[\frac{J}{\pi n} \sin \frac{\pi n}{J}\right]^2$$

The harmonic representation is thereby converted to a function connecting the calculated points, F_j at Ψ_j, by straight lines. The exact representation requires an infinite series, so truncating the series has a smoothing effect. More importantly, it can be seen that this factor decreases the magnitude of the harmonics of the least squares representation. Effectively, the rise time of the function is now restricted to at least the azimuth increment, $2\pi/J$, in the harmonic representation.

The use of harmonic analysis gives a smooth distribution of the airloads, which are actually calculated only at discrete points around the azimuth. This smoothed loading distribution then gives the blade motion through the equations of motion. The use of harmonic analysis has an important consequence in the stall model however. In the stall model described above, the lift and moment coefficients jump immediately to the stall values when the section angle of attack exceeds the dynamic stall angle. The use of harmonic analysis smooths this jump over the azimuth increment,

$2\pi/J$, which becomes a lower bound on the rise time of the stall loads. With a small azimuth increment, it is necessary to include in the stall model itself a restriction on the rise time of the stall loads (as in Section 2.1.3).

2.5.3 The Solution for First Harmonic Flapping

Since the natural frequency of an articulated blade with zero flapping hinge offset is exactly 1/REV, the equation of rigid flapping motion is singular for the solution for β_1. For n = 1 the equation, with the integral replaced by a sum over the blade span, reduces to:

$$\left(\sum_{span} r \frac{L}{4\pi b} \Delta r \right)_1 = 0$$

which is to be solved for β_1. The values of L over the disk are known, calculated at each azimuth station using some β_{1j} and β_{oj}. The solution will be found for β_1 assuming that the contributions to L from all factors except those involving β_{1j} and β_{oj} will be the same for the new values of β_1 and β_o. That is, factors such as changes in the loads due to the changes in the downwash associated with the new values of β_1 and β_o are considered as second order effects. These and similar effects, such as changes in stall region boundaries, and changes in the pitch motion, will show up eventually of course, so that the solution for a new β_1 and β_o must be obtained at each azimuth station as the calculation procedure goes around the disk, until they converge to the correct values.

These contributions to L that are assumed to be independent of β_1 and β_o are contained in the quantity

$$\left(\sum_{span} r \frac{L}{4\pi b} \Delta r \right)_{1,\,present}$$

where the subscript "present" means based on the old values of β, that is on β_{1j} and β_{oj}. This is the quantity usually used on the right hand sides of the equations of motion in the solution for the harmonics of the blade motion. From this must be subtracted the contributions due to β_{1j} and β_{oj}. The direct dependence of L on β enters only through the lifting line theory results, and since this dependence is linear, may write

$$r\frac{L}{4\pi b}\Delta r = \ell^* + \ell_{\beta_{-1}}\beta_{-1} + \ell_{\beta_1}\beta_1 + \ell_{\beta_o}\beta_o$$

where $\ell^*, \ell_{\beta_{-1}}, \ell_{\beta_1}, \ell_{\beta_o}$ are functions of r and Ψ; $\ell_{\beta_{-1}}, \ell_{\beta_1}, \ell_{\beta_o}$ are given by the lifting line theory and ℓ^* includes all other loads.

Thus the equation to be solved becomes:

$$0 = \left(\sum_{span} r\frac{L}{4\pi b}\Delta r\right)_1$$

$$= \left(\sum_{span} r\frac{L}{4\pi b}\Delta r\right)_{1,\,present}$$

$$+ \frac{1}{J}\sum_{azimuth}\sum_{span}\left\{\begin{array}{l}(\beta_o-\beta_{oj})\ell_{\beta_o} \\ +2\,Real[(\beta_1-\beta_{1j})\ell_{\beta_1}]\end{array}\right\}e^{-i\Psi_j}$$

where as before the subscript "j" refers to the sum over the azimuth (which enters in obtaining the first harmonic of $\left(\sum_{span} r(L/4\pi b)\Delta r\right)$). The solution of this equation is:

$$\beta_1 = -\frac{1}{2\Delta}\left[(Re\,S1 + Im\,S2) + i(Re\,S3 + Im\,S4)\right]$$

where

$$\Delta = S4 * S1 - S2 * S3$$

$$Re = \text{Real}(B)$$

$$Im = \text{Imaginary}(B)$$

$$B = \left(\sum_{span} r \frac{L}{4\pi b} \Delta r\right)_{i,j\,present} + \beta_0 (S6 - iS5)$$

$$- \frac{1}{J} \sum_{azimuth} \sum_{span} \left\{\beta_{0j} \ell_{\beta_0} + 2\,\text{Real}(\beta_{1j} \ell_{\beta_1})\right\} e^{-i\Psi_j}$$

and

$$S1 = \frac{1}{J} \sum_{azimuth} \sum_{span} \sin\Psi_j \; \text{Imaginary}(\ell_{\beta_1})$$

$$S2 = \frac{1}{J} \sum_{azimuth} \sum_{span} \cos\Psi_j \; \text{Imaginary}(\ell_{\beta_1})$$

$$S3 = \frac{1}{J} \sum_{azimuth} \sum_{span} \sin\Psi_j \; \text{Real}(\ell_{\beta_1})$$

$$S4 = \frac{1}{J} \sum_{azimuth} \sum_{span} \cos\Psi_j \; \text{Real}(\ell_{\beta_1})$$

$$S5 = \frac{1}{J} \sum_{azimuth} \sum_{span} \sin\Psi_j \; \ell_{\beta_0}$$

$$S6 = \frac{1}{J} \sum_{azimuth} \sum_{span} \cos\Psi_j \; \ell_{\beta_0}$$

and the solution for β_o is given as usual by

$$\beta_o = \left(\sum_{span} r \frac{L}{4\pi b} \Delta r\right)_{o,\ present}$$

Now ℓ_{β_o} and ℓ_{β_1} are given by lifting line theory if the flow is attached. Extracting the terms proportional to β_1, β_{-1}, and β_o, including the component of the downwash ($-\mu\beta_{1c}$) due to the tilt of the tip path plane with respect to the no feathering plane, gives:

$$\ell_{\beta_o} = \frac{r\Delta r}{\sqrt{1-M_N^2}} \left[\begin{array}{l} \mp \frac{1}{2} u_T (\mu \cos\psi - \frac{1}{2} b) \\ + \frac{1}{4} b (u_T + \mu \sin\psi) \end{array} \right]$$

$$\ell_{\beta_1} = \frac{r\Delta r}{\sqrt{1-M_N^2}} \left[\begin{array}{l} \pm \frac{1}{2} u_T \left[\mu - (ir + \mu\cos\psi \right. \\ \qquad \left. + b(\mp 1 - \frac{1}{2}))e^{i\psi} \right] \\ -i \frac{b}{2} e^{i\psi} \left[\mu \cos\psi - \frac{1}{2} b \right] \end{array} \right]$$

if the flow is attached, and

$$\ell_{\beta_o} = \ell_{\beta_1} = 0$$

if the flow is nonattached.

With the straight line rather than the least squares representation in the harmonic analysis, it is necessary to replace the factor 1/J by the factor:

$$\frac{1}{J} \left[\frac{J}{\pi} \sin \frac{\pi}{J} \right]^2$$

where it appears in the above.

SECTION 3

RESULTS

3.1 Effect of Dynamic Stall on the Blade Torsional Motion

Reference 5 reports the results of using the aerodynamic model described in Section 2 to calculate the airloading and blade torsional of a helicopter rotor at high advance ratio. These results may be summarized as follows.

For $0.4 < \mu < 0.8$, a stall region appears on the retreating side of the disk, outside the reverse flow region. The blade pitch motion is characterized by an initial nose-down impulse due to dynamic stall, a decrease in pitch in the fourth quadrant as increasing dynamic pressure increases the moment due to separated flow, and dynamic overshoot and damped oscillations in the first quadrant after flow reattachment occurs. The pitch oscillations are well damped by potential flow aerodynamic moments. For forward disc inclination, the stall area appears initially at outboard blade stations, resulting in larger stall moments and pitch motions.

For $\mu > 0.8$, the blade stalls before entering and after leaving the reverse flow region, which occupies a large part of the retreating side of the disk. For an articulated blade, stall is not an important feature of the loads at extremely high advance ratio, because the large collective pitch necessary to get significant stall regions results in unusably small or even negative rotor thrust.

For $\mu > 0.6$, the blade pitch motion is characterized by a large pitch increase and decrease centered about $\psi = 270$ degrees, caused by the downward lift force in the reverse flow region acting at the three-quarter chord.

The importance of the concept of dynamic stall for a rotor operating at high advance ratio lies in the fact that the rotor blade stalls at high values of the parameter $\dot{\alpha}^{(s)}c/V$, resulting

in lift and moment initially several times larger than the corresponding static stall values. It should be noted also that the dynamic overshoot due to flow reattachment following stall often is the greatest blade motion due to stall, and the severity of these oscillations is likely to be lessened only by an increase in pitch damping, possibly by mechanical means.

A presentation of the airloads and pitch motion for a rotor in various operating conditions may be found in Reference 5.

3.2 A Comparison with Experiment

Reference 9 presents limited experimental data on the torsional motion of a rotor blade in several operating conditions. The theoretical torsional motion was calculated for these cases using the model described in Section 2.

Figure 5 shows the pitch motion for $\mu = 0.68$, $i = 0$, and $\theta^\circ = 4.0$ degrees with the blade center of gravity at the 30 percent chord. This is a case of classical flutter due to center of gravity-elastic axis offset. Figure 6 shows the pitch motion for $\mu = 1.47$, $i = 0$, and $\theta^\circ = 2.0$ degrees. This is a case with large pitch motion due to the lift in the reverse flow region. For both of these cases, no elastic pitch motion was allowed.

Figure 7 shows the pitch motion for $\mu = 0.294$, $i = 0$, and $\theta^\circ = 11.0$ degrees. This is a case involving dynamic stall of the blade on the retreating side of the disk. Two theoretical results are shown: one for $\alpha_{DS} = 14$ degrees and no elastic pitch motion; and one for $\alpha_{DS} = 16$ degrees, delayed by $\Delta\psi = 20$ degrees (the abscissa for this line is actually $\psi + 20^\circ$), with no rigid pitch motion and an elastic pitch mode shape $\xi = \sin \frac{\pi}{2} r$.

A discussion of these results may be found in Reference 10. With so little experimental data it is not actually possible to make an adequate evaluation of the dynamic stall model used here.

3.3 The Effect of the Dynamic Stall Angle

The dynamic stall concept suggests a means to lessen the effects of stall. An increase in the dynamic stall angle will result in a significant reduction in the severity of the pitch motions due to dynamic stall; indeed, for a given collective pitch, a large enough dynamic stall angle could prevent the occurrence of stall at all. The dynamic stall angle is dependent on the parameter $\dot{\alpha}^{(s)}c/V$, on airfoil heaving motion, and on airfoil shape (References 3 and 4), and thus airfoils may be designed with the aim of minimizing stall effects.

In order to evaluate the effect of increasing the dynamic stall angle, the blade pitch motion was calculated for the same rotor used in the calculations of Reference 5, with several values of α_{DS}. The natural pitch frequency, ω_o, was 5.5/REV. Figures 8, 9, and 10 show the harmonics of the rigid pitch motion, θ_n (for simplicity, no elastic pitch motion was considered) for three operating conditions: Figure 8 is for $\mu = 0.5$, $i = 0$, and $\theta° = 12$ degrees; Figure 9 is for $\mu = 0.5$, $i = 0$, and $\theta° = 15$ degrees; and Figure 10 is for $\mu = 0.3$, $i = 0$, and $\theta° = 11$ degrees. Figure 11 shows the actual pitch motion for the same case as in Figure 10. The decrease in the amplitude of the pitch motion as the dynamic stall angle is increased is quite substantial.

SECTION 4

CONCLUSION

An aerodynamic and dynamic model has been constructed which has proved useful in calculating the torsional motion of a helicopter rotor blade under operating conditions involving blade stall. The concept of dynamic stall and the use of the experimental and theoretical data on dynamic stall are important parts of the aerodynamic model used here. It is clear that further work should be done to determine the nature of dynamic stall, in order that a refined, and therefore more widely applicable, model of stall may be constructed; it should be relatively simple to incorporate new data into the calculation procedure described here. There is also a great need for more experimental data on the torsional motion of rotor blades, in order that the model constructed may be rationally evaluated. Calculations of the harmonics of the pitch motion for varying dynamic stall angle have shown that the amplitude of the torsional motion is significantly decreased by an increase of the stall angle. This illustrates the value of designing airfoils for good stall characteristics.

REFERENCES

1. Ham, N.D., and Young, M.I., "Limit Cycle Torsional Motion of Helicopter Blades Due to Stall," Journal of Aircraft, Vol. 3, No. 3, May-June 1966.

2. Ham, N.D., "Stall Flutter of Helicopter Rotor Blades: A Special Case of the Dynamic Stall Phenomenon," Journal of the American Helicopter Society, Vol. 12, No. 4, October 1967.

3. Ham, N.D., and Garelick, M.S., "Dynamic Stall Considerations in Helicopter Rotors," Journal of the American Helicopter Society, Vol. 13, No. 2, April 1968.

4. Ham, N.D., "Aerodynamic Loading on a Two-Dimensional Airfoil During Dynamic Stall," AIAA Journal, Vol. 6, No. 10, October 1968.

5. Johnson, Wayne, "The Effect of Dynamic Stall on the Response and Airloading of Helicopter Rotor Blades," Journal of the American Helicopter Society, Vol. 14, No. 2, April 1969.

6. Halfman, R.L., Johnson, H.C., and Haley, S.M., "Evaluation of High Angle of Attack Aerodynamic Derivative Data and Stall Flutter Prediction Techniques," NACA TN 2533, November 1951.

7. Critzos, C.C., Heyson, H.H., and Boswinkle, R.W., Jr., "Aerodynamic Characteristics of NACA 0012 Airfoil Section at Angles of Attack from 0 Deg to 180 Deg," NACA TN 3361, 1955.

8. Miller, R.H., and Ellis, C.W., "Helicopter Blade Vibration and Flutter," Journal of the American Helicopter Society, Vol. 1, No. 3, July 1956.

9. Niebanck, C.F., "A Comparison of Dynamically Scaled Rotor Test Data with Discrete Azimuth Aeroelastic Stability Theory," Proceedings of the 25th Annual Forum of the American Helicopter Society, May 1969.

10. Ham, N.D., and Johnson, Wayne, "A Comparison of Dynamically Scaled Rotor Test Data with a Step-by-Step Calculation of Rotor Blade Torsional Motion," Proceedings of the 25th Annual Forum of the American Helicopter Society, May 1969.

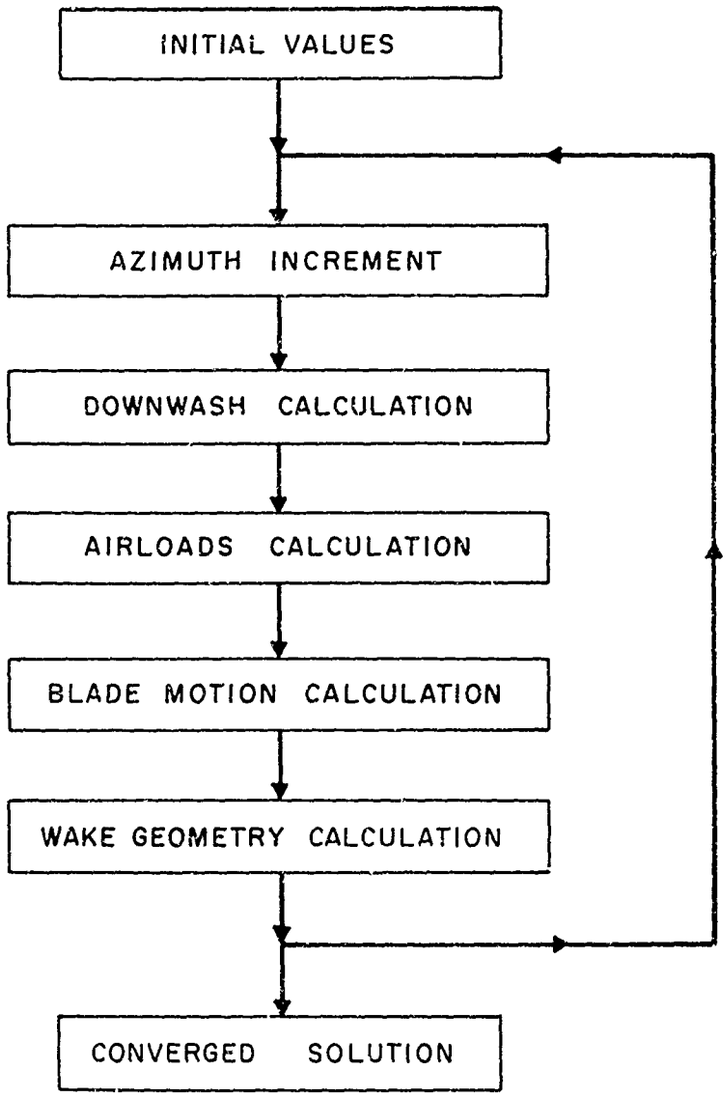

FIGURE 1 PROCEDURE FOR CALCULATION OF ROTARY WING AIRLOADS

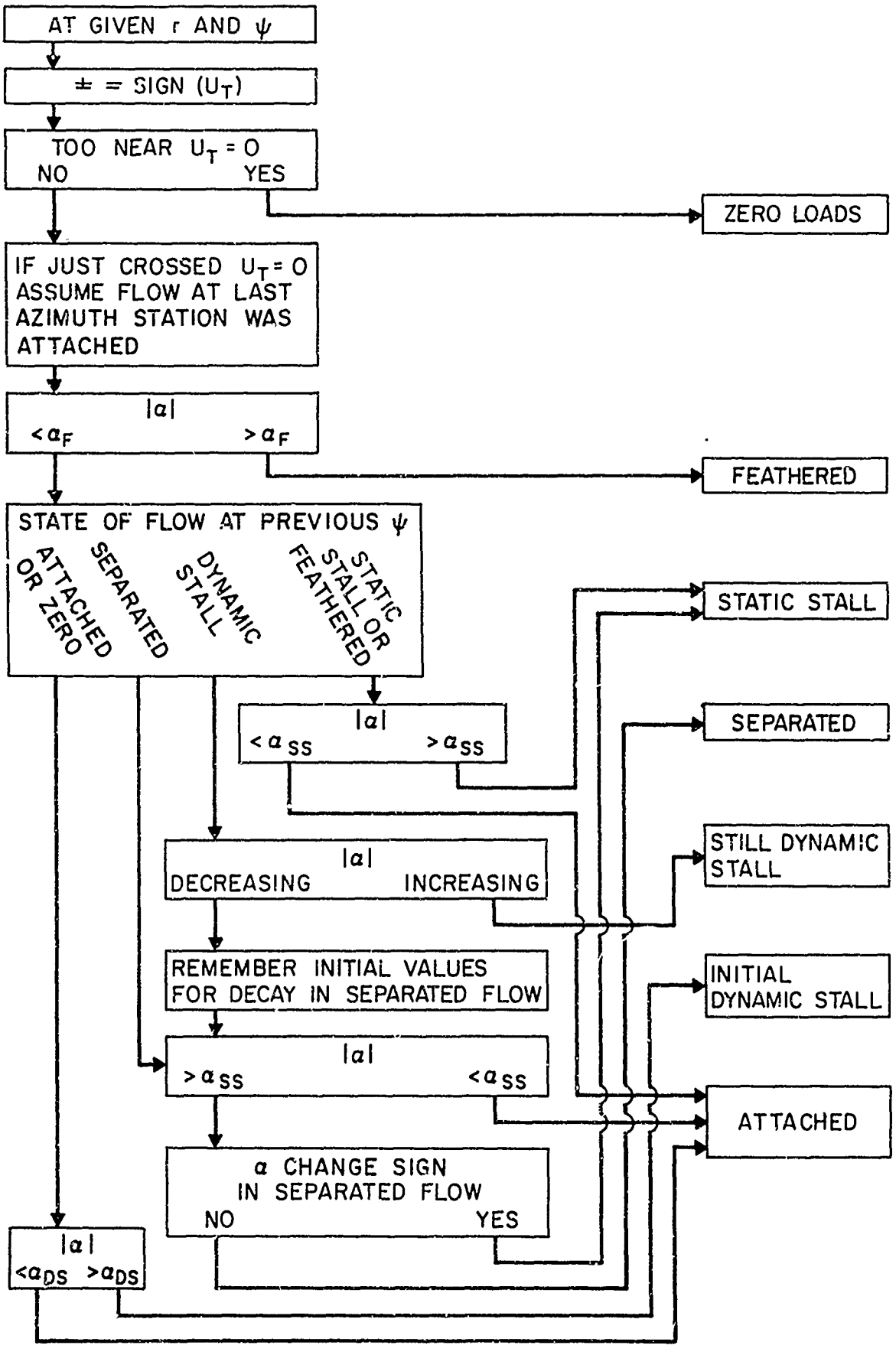

FIGURE 2 THE SECTION LOADS CALCULATION

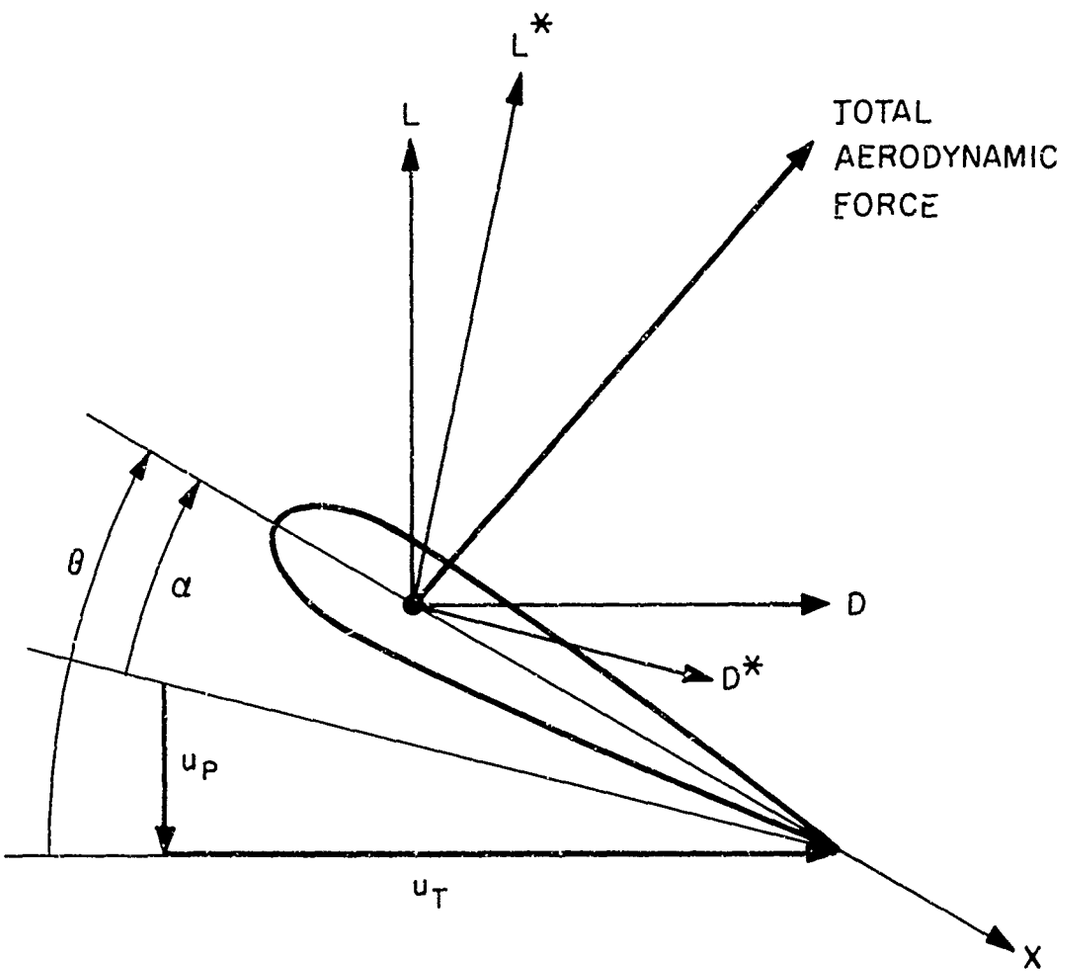

FIGURE 3. GEOMETRY OF THE BLADE SECTION

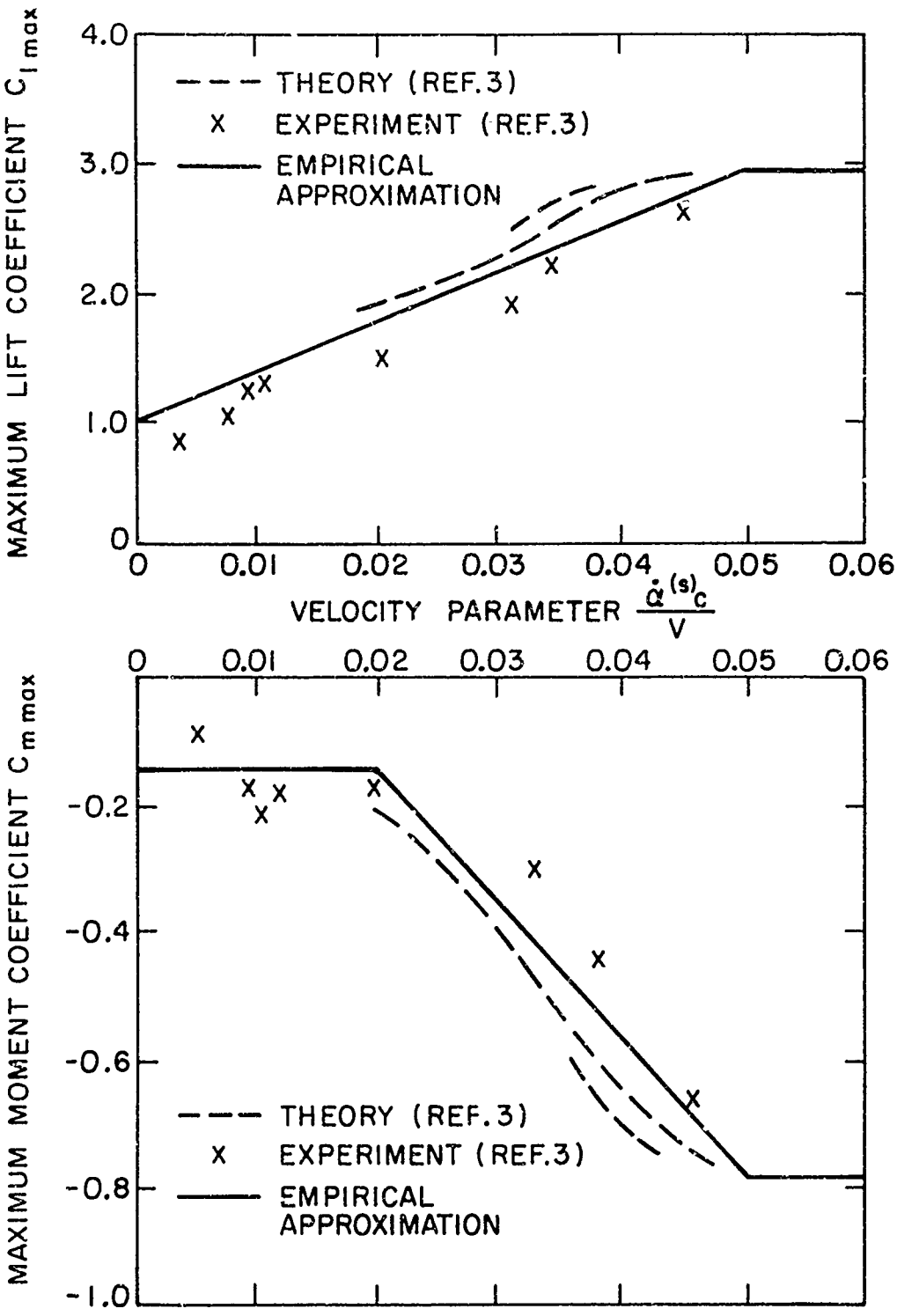

FIGURE 4. MAXIMUM LIFT AND MOMENT COEFFICIENT VERSUS RATE OF CHANGE OF ANGLE OF ATTACK

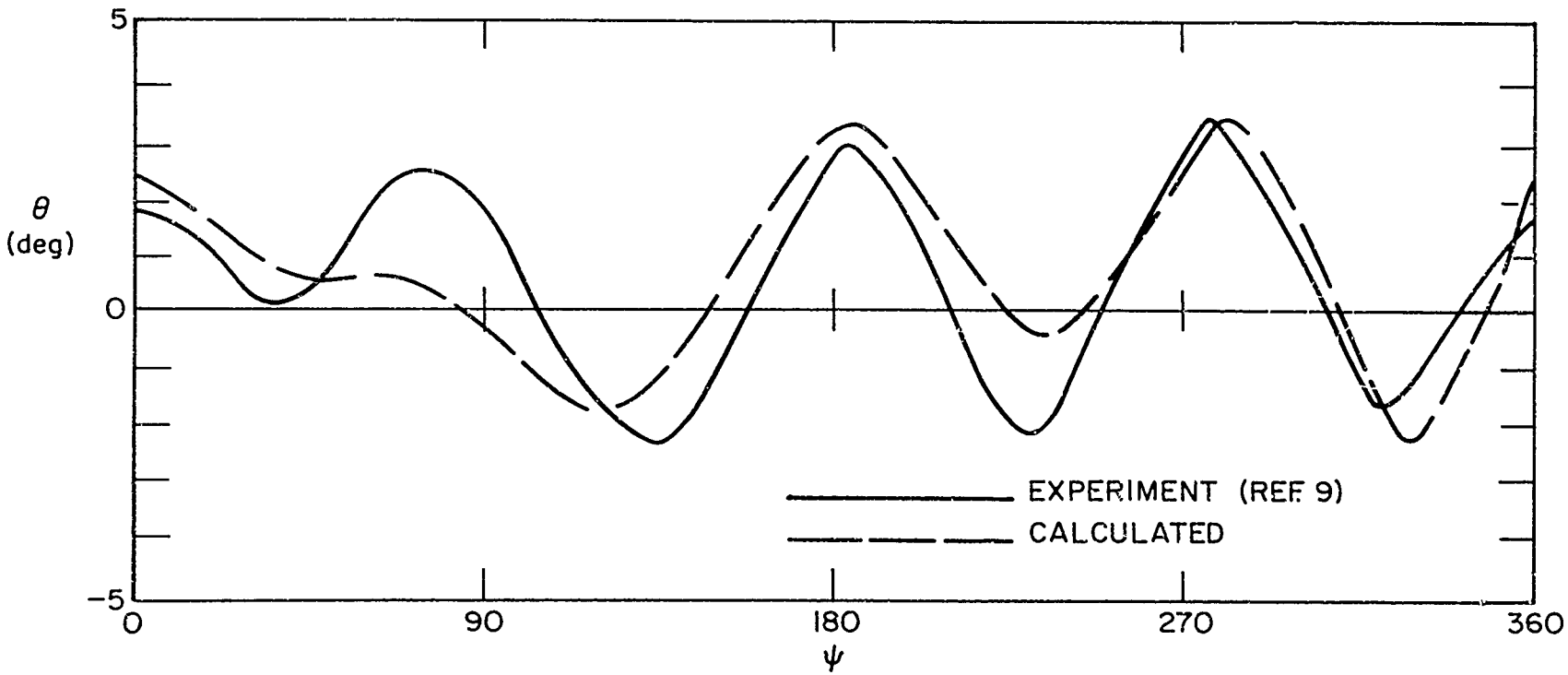

FIGURE 5 BLADE PITCH MOTION: $\mu = 0.5$, $i = 0$, $\theta^\circ = 4$, AND BLADE CENTER OF GRAVITY AT 0.30 CHORD

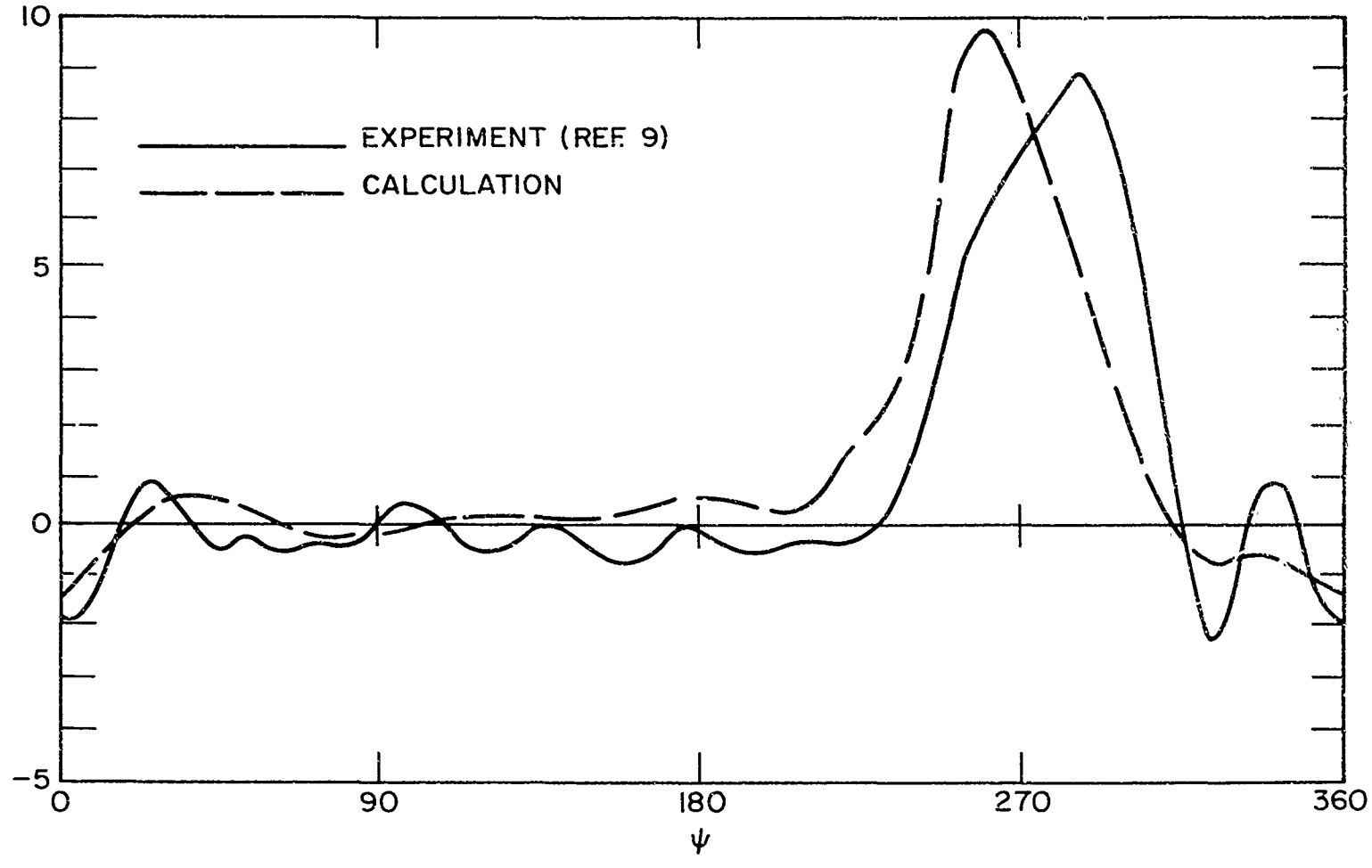

FIGURE 6 BLADE PITCH MOTION: $\mu = 1.47$, $i = 0$, $\theta^\circ = 2$

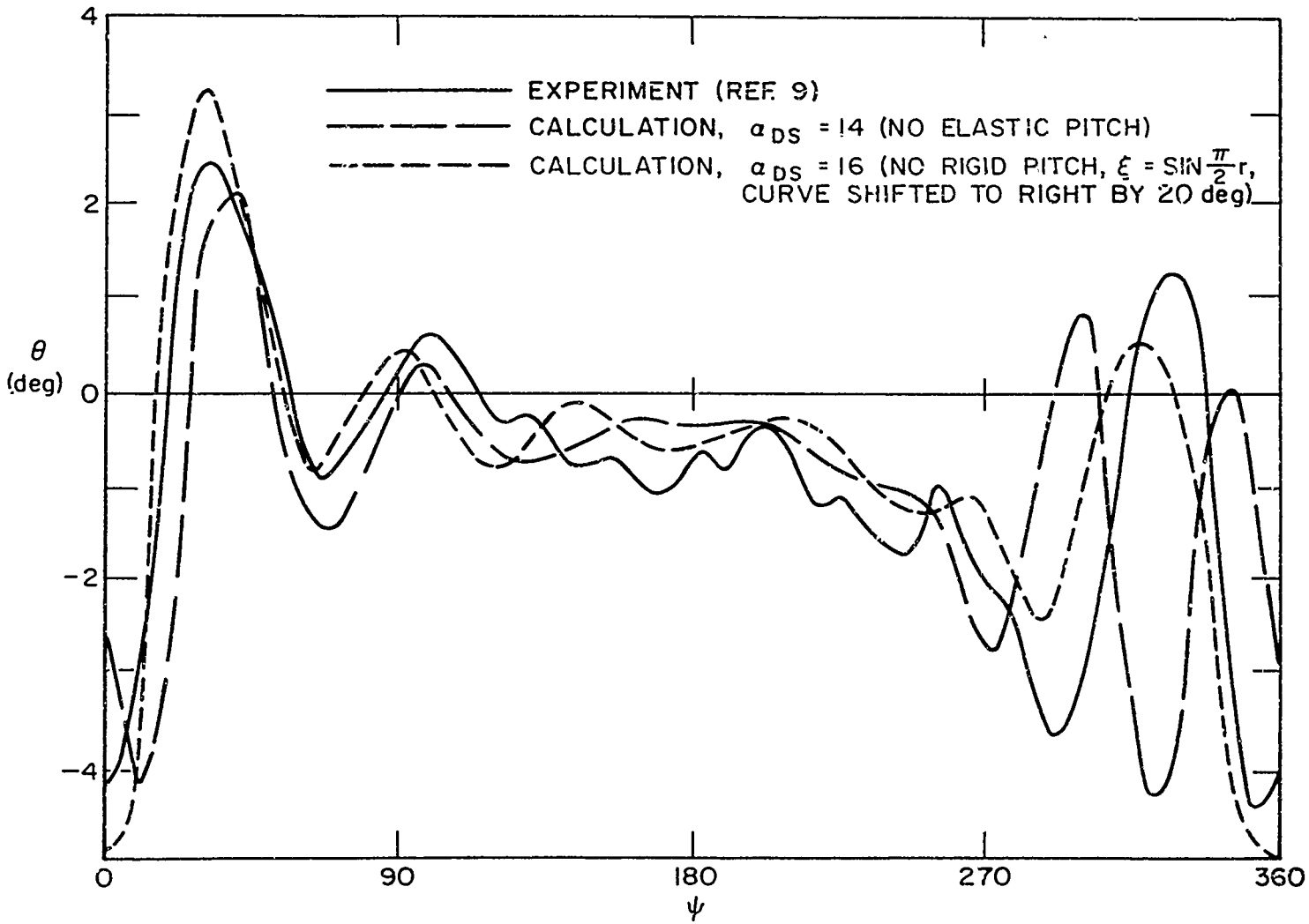

FIGURE 7 BLADE PITCH MOTION: μ=0.294, i = 0, θ° = 11

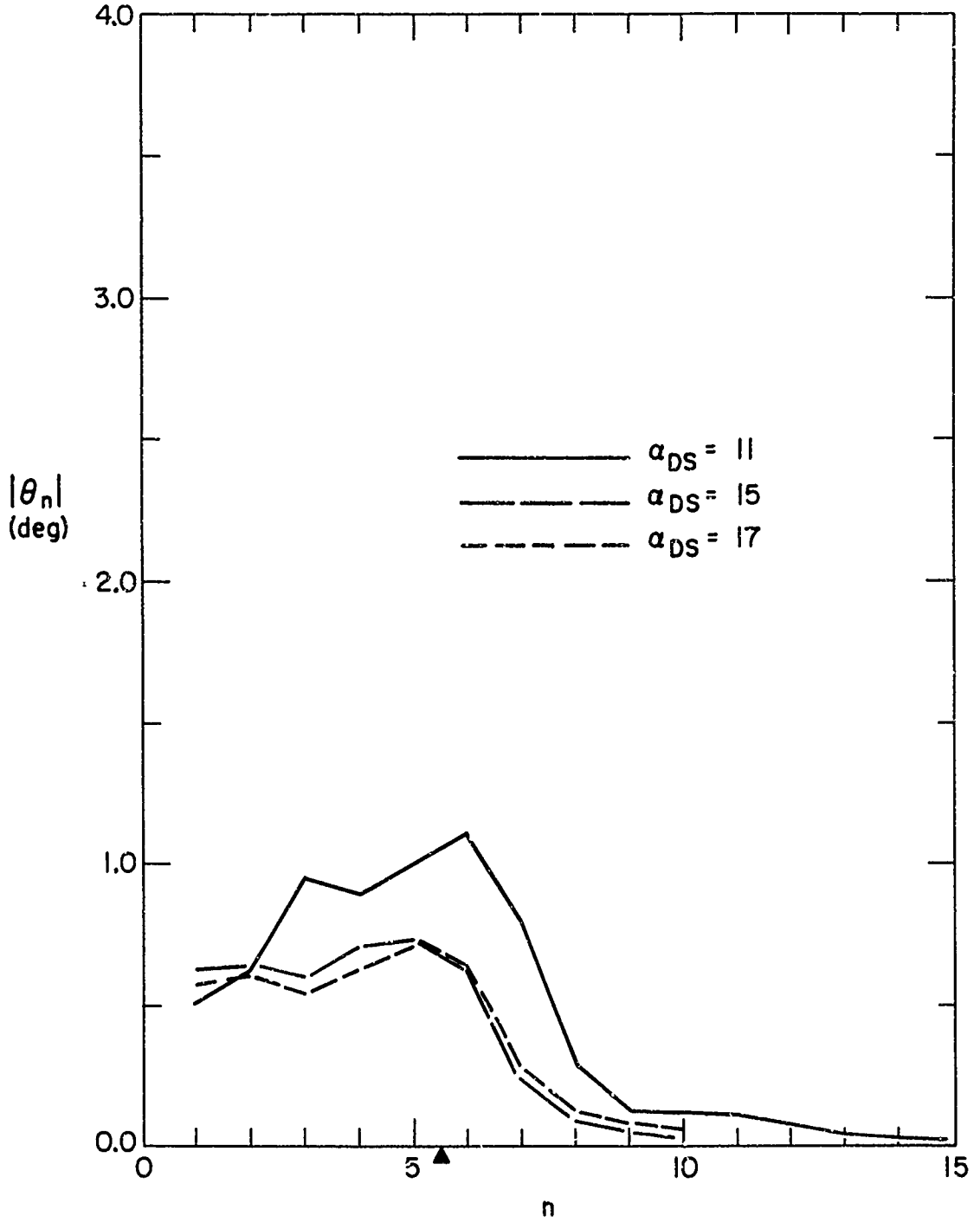

FIGURE 8 HARMONICS OF PITCH MOTION FOR VARYING DYNAMIC STALL ANGLE : $\mu = 0.5$, $i = -5$, $\theta^\circ = 12$, $C_T/\sigma = 0.052$

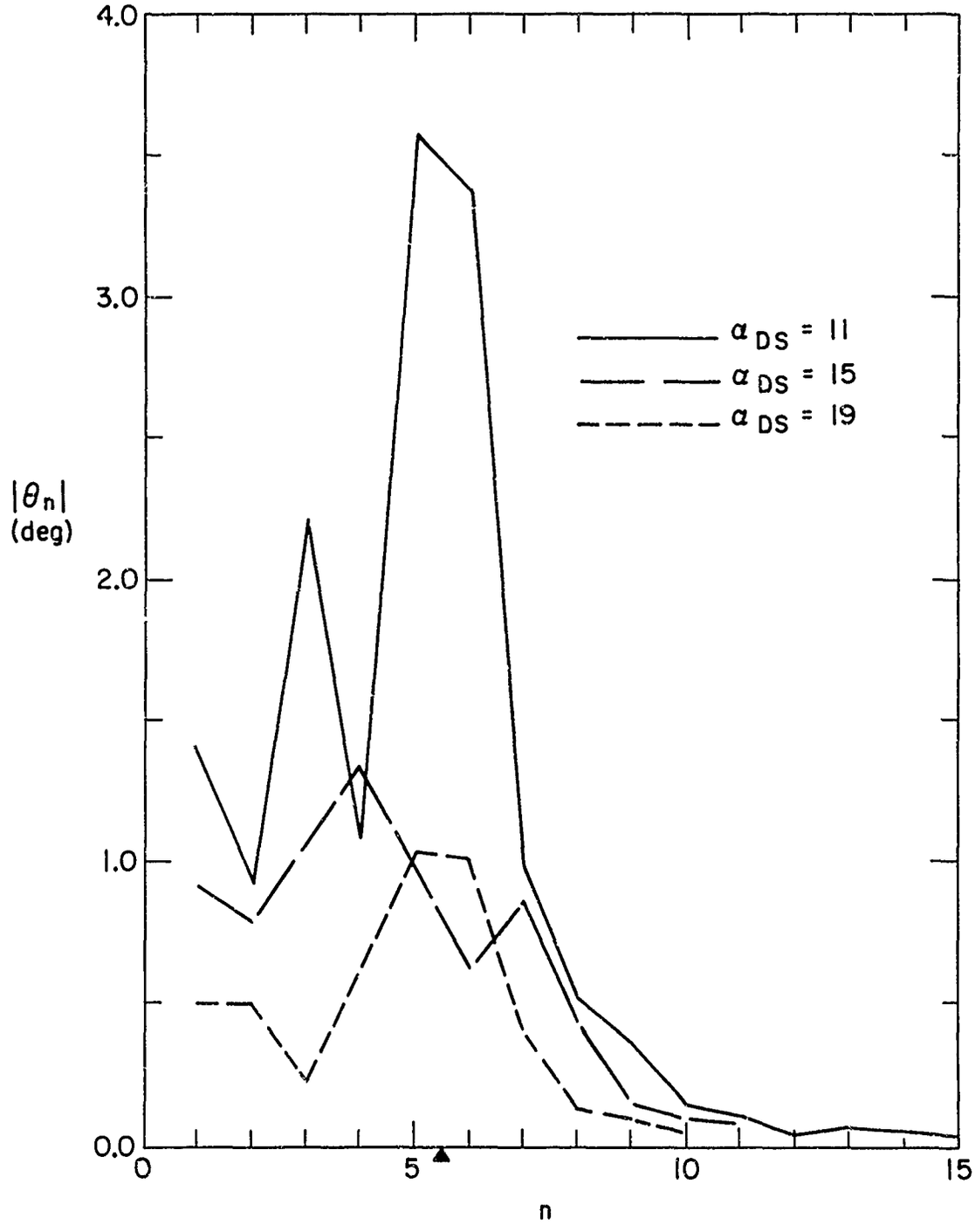

FIGURE 9 HARMONICS OF PITCH MOTION FOR VARYING DYNAMIC STALL ANGLE: $\mu = 0.5$, $i = -5$, $\theta^\circ = 15$, $C_T/\sigma = 0.070$

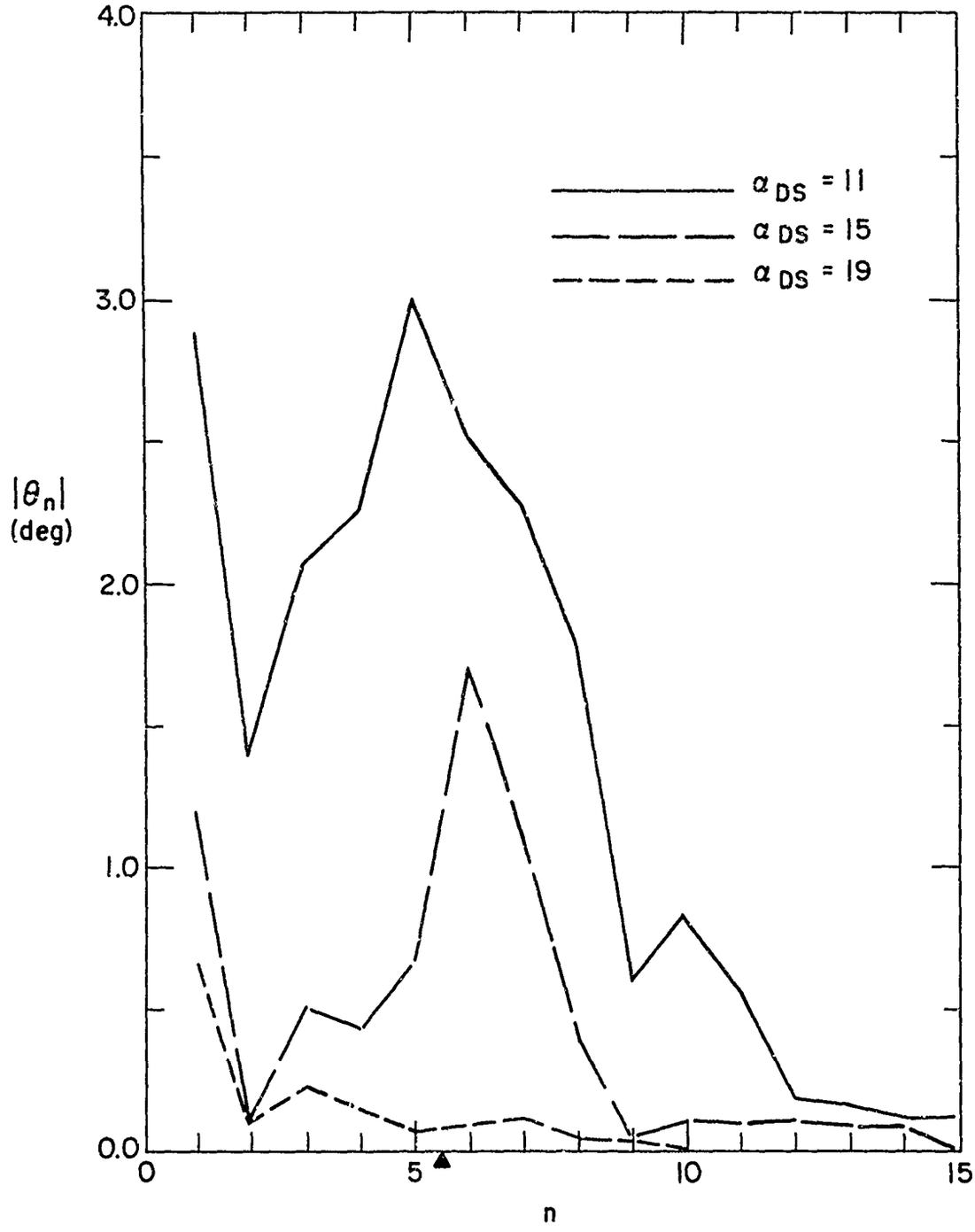

FIGURE 10 HARMONICS OF PITCH MOTION FOR VARYING DYNAMIC STALL ANGLE: μ= 0.3, i= 0, θ°= 11, C_T/σ = 0.104

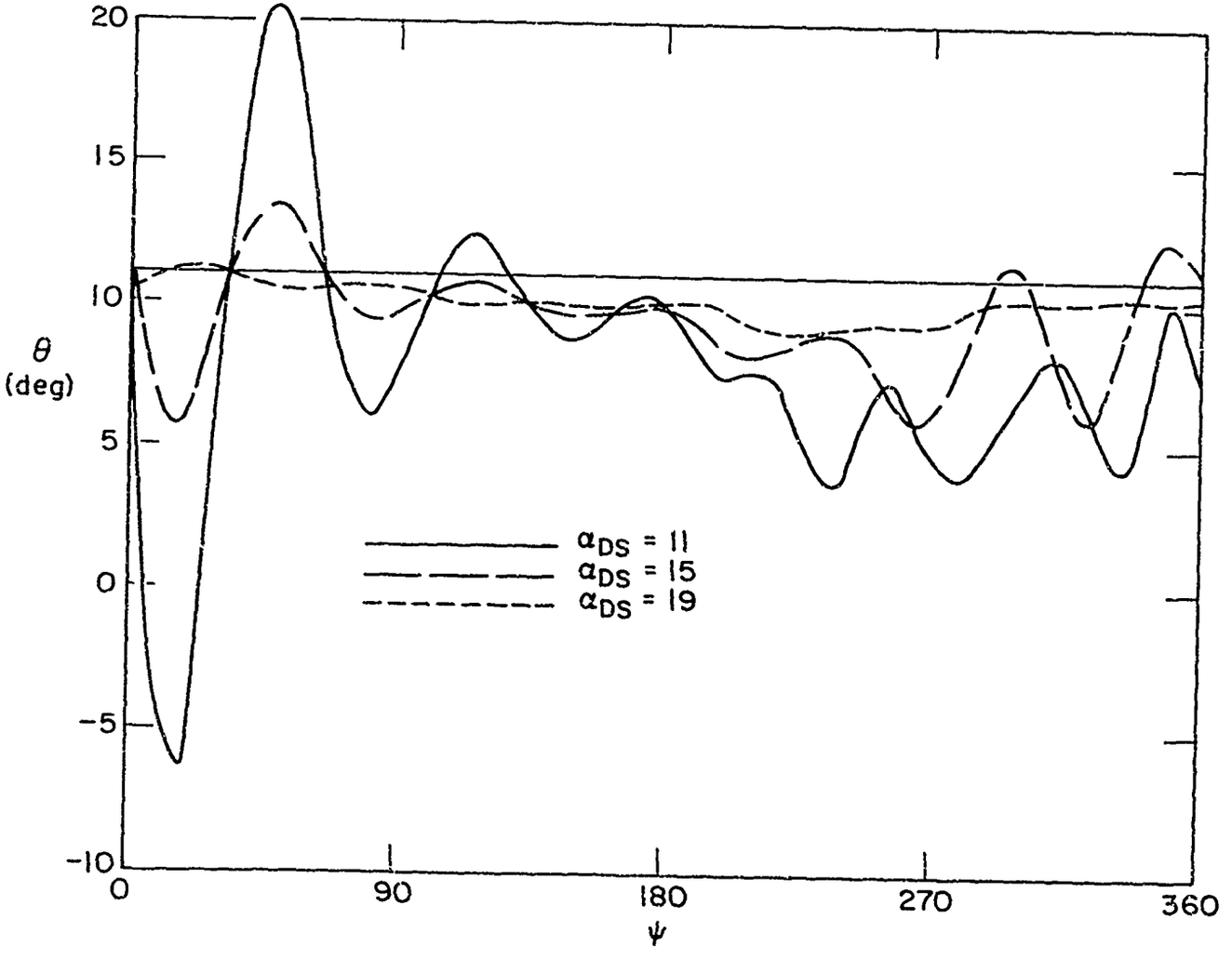

FIGURE 11 PITCH MOTION FOR VARYING DYNAMIC STALL ANGLE: μ= 0.3, i = 0, θ°= 11, C_T/σ = 0.104

UNCLASSIFIED

Security Classification

DOCUMENT CONTROL DATA - R & D

Security classification of title, body of abstract and indexing annotation must be entered when the overall report is classified)

1 ORIGINATING ACTIVITY (Corporate author) Massachusetts Institute of Technology Aeroelastic & Structures Research Laboratory Cambridge, Massachusetts 02139	2a. REPORT SECURITY CLASSIFICATION UNCLASSIFIED 2b. GROUP

3 REPORT TITLE

The Response and Airloading of Helicopter Rotor Blades Due to Dynamic Stall

4 DESCRIPTIVE NOTES (Type of report and inclusive dates)

Technical Report

5 AUTHOR(S) (First name, middle initial, last name)

Wayne Johnson

6 REPORT DATE May 1970	7a. TOTAL NO OF PAGES 44	7b. NO. OF REFS 10
8a. CONTRACT OR GRANT NO DA-31-124-ARO-D-247 b. PROJECT NO c. d.	9a. ORIGINATOR'S REPORT NUMBER(S) ASRL TR 130-1 9b. OTHER REPORT NO(S) (Any other numbers that may be assigned this report)	

10 DISTRIBUTION STATEMENT

This document has been approved for public release and sale; its distribution is unlimited.

11 SUPPLEMENTARY NOTES	12 SPONSORING MILITARY ACTIVITY U.S. Army Research Office-Durham

13 ABSTRACT

An aerodynamic model is constructed for the application of the properties of dynamic stall of airfoils to the calculation of the airloads and blade motion of helicopter rotor blades. Dynamic stall occurs on an airfoil undergoing pitching motion at high angle of attack, and is characterized by peak section lift and moment much larger than the corresponding static stall loads. A method is developed for the solution of the equations of motion of a rotor blade by means of harmonic analysis. The effect of dynamic stall on the blade torsional motion at high advance ratio is examined, and comparison is made with the limited experimental data available. An increase in the dynamic stall angle is shown to significantly decrease the amplitude of the pitch motions.

DD FORM 1 NOV 65 1473

UNCLASSIFIED

Security Classification

14 KEY WORDS	LINK A		LINK B		LINK C	
	ROLE	WT	ROLE	WT	ROLE	WT
dynamic stall						
helicopter airloads						
rotor blade motion calculation						
rotor blade torsional motion						